Appl. Magn. Reson. 18, 493–503 (2000)

Applied Magnetic Resonance

In Situ Conduction ESR and Theoretical Studies of Graphite Intercalation by Nitric Acid*

A. M. Ziatdinov and P. G. Skrylnik

Institute of Chemistry, Russian Academy of Sciences,
Vladivostok, Russian Federation

Received October 31, 1999; revised December 28, 1999

Abstract. Results of an in situ conduction electron-spin resonance (CESR) study of HNO_3 molecule intercalation into highly oriented pyrolytic graphite (HOPG) plate with width being comparable with the graphite skin-depth governed by the c-axis conductivity are presented. The changes in the graphite CESR signal line shape, intensity and linewidth and the stepwise changes both of intensity and linewidth of CESR signal of intercalated sample were clearly detected during this reaction. Under the assumption that the graphite CESR signal evolution is caused by the advance of a boundary separating the intercalated and nonintercalated HOPG, the average value of spin reorientation probability during the collision of current carriers with this interface and the diffusion coefficient of nitric acid into the HOPG plate were extracted from experimental data. With the chemical potential versus intercalation time proposed by the authors for the experimental conditions, the stepwise changes of the CESR signal intensity of intercalated sample was calculated theoretically.

1 Introduction

In spite of numerous publications devoted to studies of various aspects of the structure and properties of graphite intercalation compounds (GICs) [1–3], hitherto many aspects of the mechanism of intercalation of "guest" molecules into graphite have not received sufficient attention. Conduction electron-spin resonance (CESR) technique is one of the most powerful methods for studying the graphite intercalation process because the shapes and intensities of the CESR signal both of nonintercalated and intercalated regions of graphite plate vary strongly during the intercalation. However, because of the difficulty to conduct reproducible experiments only a few CESR studies of the graphite intercalation process have been undertaken [4–9]. But even in these cases, due to the presence of a skin-effect the interpretation of changes in the graphite CESR signal during the intercalation

* Presented at the 2nd Asia-Pacific Symposium, Hangzhou, China, October 31 to November 4, 1999.

process comes across greater difficulties. This paper presents the results of an in situ CESR study of intercalation of HNO_3 molecules into highly oriented pyrolytic graphite (HOPG) plate with a width which is comparable with the graphite skin-depth δ_c governed by the c-axis conductivity σ_c and discusses in a theoretical analysis the CESR signal parameter evolution, including reasons for a stepwise increase with time of the CESR signal intensity from the intercalated graphite plate.

2 Experimental

CESR measurements were carried out at room temperature on an X-band E-line spectrometer. The constant magnetic field (H_0) modulation frequency and amplitude were 2.5 kHz and 0.1 mT, respectively. The experiments were carried out on HOPG plates with height (h)×width (l)×thickness (d) = 0.4×0.04×0.02 cm^3, where $h \times l$ are dimensions of the basal plane. The HOPG samples were held in a quartz tube connected via a valve to the reservoir with intercalate (liquid HNO_3 with density $\rho \cong 1.565$ g/cm^3). Nitric acid vapor penetrated into the knee of reactor with the graphite sample through a hole with a size of ca. $8 \cdot 10^{-3}$ cm^2 in the fluoroplastic diaphragm. Prior to the experiment, the system was evacuated to eliminate air and water. During the measurements H_0 was applied along the graphite c-axis. The basal $l \times h$ and lateral $d \times h$ sides were parallel to the magnetic component H_{rf} of the microwave field. Note that in the rectangular resonator, the structure of the electromagnetic field of TE_{102} mode has such a form that, at a conventional setting of the resonator, H_0 is parallel to the electrical component E_{rf} of the microwave field (Fig. 1).

According to data of the four-probe method, at 300 K the conductivity σ_c of the HOPG plate used is equal to 7.7±0.8 $\Omega^{-1}cm^{-1}$. In the X-band experi-

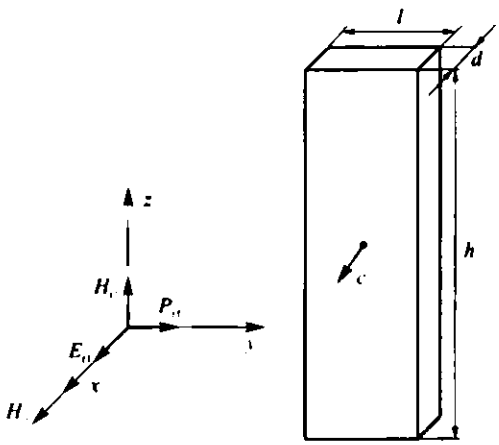

Fig. 1. Orientation of the HOPG plate with dimensions $l \times h \times d$ relative to the external constant magnetic field H_0, the electric E_{rf} and the magnetic H_{rf} components of microwave field, the Poynting vector P_{rf} and cavity axis z in an unloaded rectangular cavity.

ment the value $\delta_c \sim l/2$ corresponds to this conductivity, i.e., the whole volume of the HOPG plate investigated was available for the CESR studies.

3 Results

The CESR spectrum of HOPG plate consists of a single asymmetric line typical for conducting samples due to the Dyson mechanism [10]. The spectrum is axial with respect to the c-axis and is characterized by $g_\perp = 2.0474 \pm 0.0002$ and

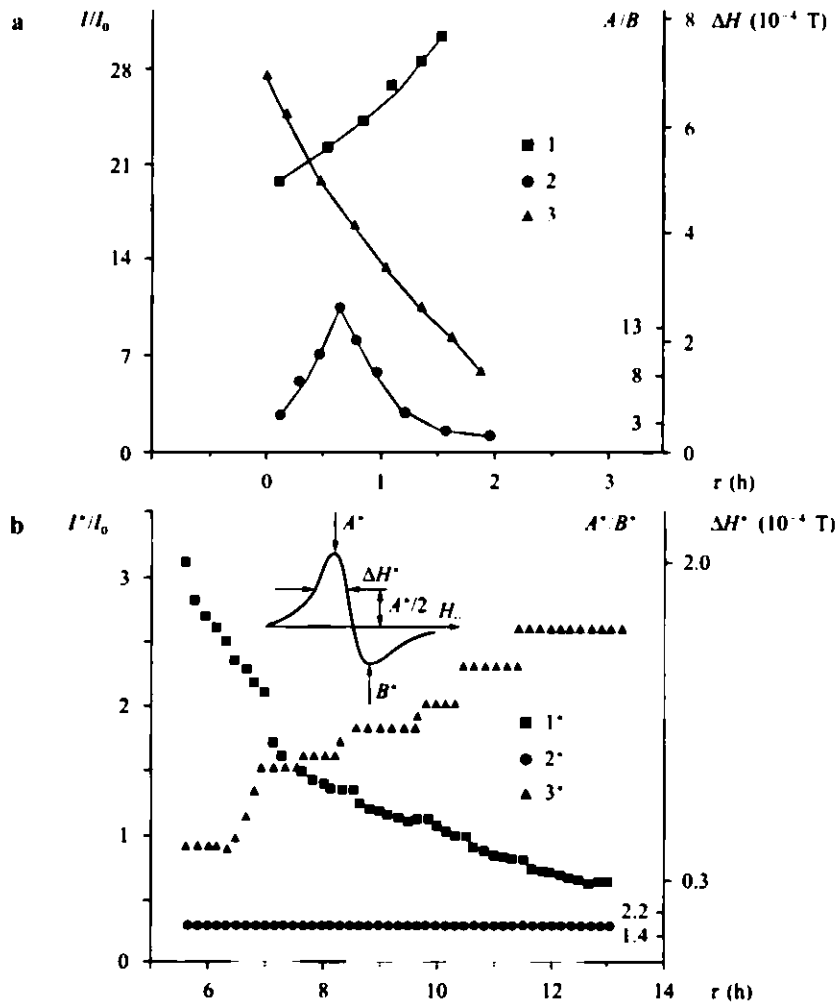

Fig. 2. CESR lineshape parameters for a nonintercalated and b intercalated parts of the narrow ($l \sim 2\delta_c$) HOPG plate vs. exposure time, t, in HNO_3 atmosphere. 1(1*), 2(2*) and 3(3*) correspond to ΔH (ΔH^*), A/B (A^*/B^*) and I/I_0 (I^*/I_0), respectively. I [I^*] = $(A + B)\Delta H^2$ [$(A^* + B^*)\Delta H^{*2}$]; I_0 is the intensity of the standard ESR signal.

$g_\perp = 2.0029 \pm 0.0002$. The line asymmetry parameter, A/B, determined as the maximum-to-minimum peak height ratio, both measured with respect to the baseline of the first derivative of the CESR absorption line, is "normal" in the sense that the maximum peak height occurs at the lower magnetic field and is about 1.8.

Several minutes after the injection of HNO_3 gas into the part of the reactor with the HOPG plate, the graphite CESR signal begins to transform and decrease in intensity until it fully disappears. Simultaneously, a new signal with $g_\parallel^* = 2.0019 \pm 0.0002$, and $g_\perp^* = 2.0030 \pm 0.0002$ appears in the spectrum, where g_i^* ($i = \parallel, \perp$) is determined by the H_0 value at the point of intersection of the first derivative of the CESR absorption line and the baseline.

The linewidth (the intensity), ΔH ($I = (A + B)\Delta H^2$), of the graphite CESR signal increases (decreases) vs. exposure time, τ, monotonously (Fig. 2a). The A/B ratio of the signal increases initially, but it is still "normal" reaching a maximum A/B value of about 13. Later, upon further exposure to the intercalate atmosphere, the A/B ratio becomes "reversed" (maximum peak height, A, occurs at higher magnetic fields), and its magnitude decreases down to about 2; the A/B maximum corresponds to the moment when the phase reversal takes place (Fig. 2a). The g_i ($i = \parallel, \perp$) values of the graphite CESR signal do not change up to its disappearance.

Early in the development of the reaction, a wide scattering of the intensity, $I^* = (A^* + B^*)\Delta H^{*2}$, and the linewidth, ΔH^*, values of the CESR signal with g_i^* has been observed. As the time of reaction increases, this scattering decreases and both the I^* and ΔH^* vs. exposure time, τ, take a clearly stepwise form (Fig. 2b). The asymmetry ratio, A^*/B^*, and g_i^*-values of the signal remain constant up to the end of reaction.

4 Discussion

At a given configuration of the ESR experiment (Fig. 1) microwave field penetrates into the HOPG plate mainly through its lateral sides, which are parallel to both the c-axis and H_{rf} [11], i.e., through the lateral sides $h \times d$. Therefore, the evolution of the graphite CESR signal of the sample (Fig. 2a) is mainly due to variations of the composition and properties of the HOPG plate at the surface areas from these sides. The dependence of the shape and intensity of the graphite CESR signal on exposure time of a sample in HNO_3 vapor is qualitatively identical to that of the ESR signal lineshape and intensity of the localized spins in a metallic substrate on the thickness of a spray-coated film of another metal [12]. In our case, the spins in consideration are certainly mobile, but for the $l/\delta_c < 2$ the CESR line shape does not depend on spin mobility [13, 14], i.e., in the framework of the Dyson theory [10] in the HOPG plate the spin carriers may be considered as localized. Therefore, the variations of the shape and intensity of the graphite CESR signal may be considered as caused by the formation of a macroscopic "intercalation" layer on the HOPG substrate, and by advance of the boundary which separates the intercalated and as-yet the nonintercalated parts of sample. The invariability of g_i and g_i^* ($i = \parallel, \perp$) values up to the disappear-

ance of the graphite CESR signal and the end of reaction, respectively, indicates that the boundary may be considered as nonconductive. This may be determined by significant distortion of a carbon net near the intercalation front and/or by the presence of high phase-boundary electrostatic potential.

In the experiment under consideration the total volume of the sample is available for CESR studies. Therefore, the time of the graphite CESR signal disappearance corresponds approximately to the moment of contact of the counter (antiparallel) intercalation fronts. Let us assume that the thickness of the intercalated layer, d, depends on the exposure time as $d^2 = 2D_{int}\tau$ (where D_{int} is the intercalate two-dimensional diffusion constant). In such case, substituting the value of the time interval from the beginning of the graphite CESR signal transformation up to its disappearance, $\tau \cong 3$ h, and $d = l/2$ into this expression, it is easy to estimate the value $D_{int} \cong 1.1 \cdot 10^{-6}$ cm^2/min.

A new and unexpected result of this experiment is the significant broadening of the graphite CESR signal from the beginning of the intercalation up to the contact of the counter intercalation fronts (Fig. 2a). We suppose that the reason for it is the collisions of current carriers with the nonconductive boundary between the intercalated and the nonintercalated parts of the HOPG plate. Indeed, when the intercalation front advances inside a plate the width of its nonintercalated part decreases and hereupon a frequency of collisions of spin carriers with the aforementioned interfaces increases. Therefore, at nonzero probability of spin reorientation during such collisions, the increase of the total rate of spin relaxation of current carriers (the CESR linewidth) with the time of intercalation can be observed. Note that in all previous ESR experiments on graphite intercalation [4–9] which were carried out on HOPG plates with $l \gg \delta_c$, a similar broadening of the graphite CESR signal was not observed. This is an indirect evidence supporting the proposed interpretation of the graphite CESR signal broadening at the intercalation of the narrow ($l \sim 2\delta_c$) HOPG plate.

With the relation $\tau = d^2/2D_{int}$, the experimental dependence $\Delta H(\tau)$ (Fig. 2a) can be easily transformed into the dependence $\Delta H(a)$, where $a = l - 2d$ is the thickness of the nonintercalated part of the HOPG plate (Fig. 3). The latter dependence can be calculated theoretically as well with the Dyson theory for the CESR in metals, including the effects of surface relaxation [10]. It is assumed in this theory that an electron colliding with the surface has a certain probability ε of spin reorientation during the collision, in addition to the steady probability $1/T_2$ (T_2 is the spin-relaxation time due to the collisions of current carriers with the imperfections in the sample volume) which exists for all electrons. In the general Dyson expressions for the CESR line shape [10] the contribution of the surface spin relaxation effects into the CESR line shape is determined by the value of term $Q = 1/2g\theta$, where $g = 3\varepsilon/4\Lambda$ (Λ is a mean free path of current carriers) and θ is a sample thickness. Obviously, if ε is considered as average probability of spin reorientation of graphite current carrier during its collision with the nonconductive phase boundary then the mentioned expressions can be used for analysis of $\Delta H(a)$ dependence also. As is seen from Fig. 3, where the results of such analysis are presented, the theoretical graphite CESR line width

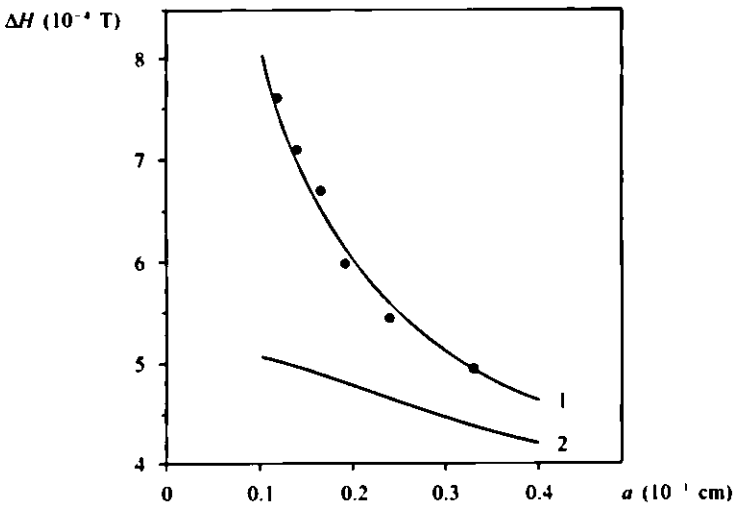

Fig. 3. Graphite CESR linewidth, ΔH, vs. thickness of the nonintercalated part of the HOPG plate $a = l - 2d$. The dots correspond to the experimental data. The lines 1 and 2 correspond to the theoretical graphite CESR linewidth calculated with the Dyson expression [10] with $g = 10$ and 0, respectively. The values of $R_s = 2.4$, $\delta_c = 2.6 \cdot 10^{-2}$ cm and $T_2 = 1.4 \cdot 10^{-8}$ s for HOPG plate intercalated, necessary for calculation of this theoretical dependence, were taken from [15].

versus $a = l - 2d$ with $g = 10$ cm^{-1} describes the experimental data well. (The HOPG values of $T_2 = 1.4 \cdot 10^{-8}$ s, T_{D_a} (the spin diffusion time across the skin-depth δ_c) $= 8 \cdot 10^{-8}$ s, and $\delta_c = 2.6 \cdot 10^{-2}$ cm which are necessary for the calculation of this dependence were taken from [15].) The found value of g and the typical HOPG values of $\Lambda = (0.4 \div 1.6) \cdot 10^{-5}$ cm [16] correspond to $\varepsilon = (0.5 \div 2.1) \cdot 10^{-4}$. For comparison, the surface spin reorientation probability of conduction electrons in Cu and Li samples are equal to $\sim 10^{-2}$ [17] and $\sim 5 \cdot 10^{-6}$ [18], respectively.

Experimental data (Fig. 2b) show that the intercalation process is not a continuous one, i.e., it has a clear stepwise shape: relatively short time intervals with sharp increase in I^* followed by the time intervals with I^* being nearly constant. This fact is in good agreement with literature data [1, 19–25] reporting that in many cases the graphite intercalation proceeds through the formation of definite intercalation stages and that the amount of intercalate inside the sample and, as a result, the current carrier concentration, increases with GIC stage index decreases. According to our X-ray diffraction data the first (last) "plateau" in experimental dependence $I^*(\tau)$ (Fig. 2b) corresponds to the seventh (second) intercalation stage. Therefore, the number of steps in the $I^*(\tau)$ dependence is equal to the number of possible intercalation stages and the stepwise increase in I^* may be attributed to the sequence of stage transitions from the stages with large integer indices to the stages with small ones. (The presence of two close steps instead of one, corresponding to the sixth stage (Fig. 2b), may be connected with the change in the stacking of graphite layers situated between the

nearest intercalate layers. First, such stacking transformation was observed in the second-stage alkali-metal-intercalated graphite by X-ray scattering measurements [26]. In $C_{s,n}HNO_3$ the stacking transformations were not investigated, but the difference in a stacking sequence in samples with even and odd stage indices was proved experimentally [27–29]. The energy barrier, associated with large-scale sliding of carbon layers at the stacking transformation, and corresponding changes in electronic structure decrease with the stage index number decreases. This reason may account for the absence of doubling the number of steps corresponding to the stages with indices $n < 6$ in the experiment considered (Fig. 2b). In the subsequent calculations we neglected splitting of the "plateau" in the $I^*(\tau)$ dependence corresponding to the sixth stage.) Under above-stated understanding of the reason for the stepwise dependence of $I^*(\tau)$, the time intervals with an invariable value of I^* correspond to the periods during which the insertion of intercalate from gas phase into the GIC plate is negligible. At this time, the concentration of current carriers in carbon layers does not change, but reorganization of intercalate subsystem continues. In particular, it is confirmed by the CESR linewidth decrease within $I^*(\tau)$ plateau (Fig. 2b). The reorganization of intercalate subsystem during considered time intervals may consist in splitting and merging of intercalate islands, at a simultaneous increase of their mean size, and in preparing other necessary conditions for the next stage transition.

In our paper for the theoretical interpretation of the observed experimental dependence, $I^*(\tau)$ analytical expressions for the stage fractions calculation by Kirczenow [30] have been utilized. In that paper an appropriate model of stage order and disorder as a result of evolution of Daumas-Herold domains during intercalation was presented. In the frameworks of that model calculation for the stage fractions f_i at given parameters (temperature, chemical potential, domain size, etc.) may be fulfilled as follows [30]:

$$f_i = \exp(c_i) \qquad \left(\sum_i \exp(c_i) = 1\right), \tag{1a}$$

$$c_i = N_0 \ln N_0 - N \ln N - (N_0 - N)\ln(N_0 - N) - \frac{i\Psi}{kT} + \frac{1}{kT}\left(\mu N + \frac{E_{\parallel} z N^2}{2N_0} - \gamma N_0 - \frac{u_i N^2}{N_0}\right). \tag{1b}$$

Equation (1b) was found from the minimization of the free energy Ψ with respect to the distributions f_i and in-plane density x of intercalate within domain ($x = N/N_0$). In Eqs. (1) N_0 is the number of lattice-gas sites available to intercalate in any gallery within domain, N is the number of sites filled with intercalate, T is temperature, k is the Boltzmann constant, μ is the chemical potential, $E_{\parallel}$ is the nearest neighbor in-plane interaction energy between intercalates, z is the in-plane coordination number, $u_i = \upsilon_0 i^{-a}$ is the repulsive interaction between intercalate layers across i carbon layers, γ is the energy per lattice-gas site which is required to separate the host layers sufficiently to admit the intercalates. Hav-

ing μ known and substituting other parameters into Eqs. (1) we can obtain filling coefficient x and distribution f_i for the possible stages i. Then, resulting values enable us to estimate the total amount of intercalate in GIC sample:

$$M = M_{\max} \sum_i f_i\left(\frac{1}{i}\right)\frac{N}{N_0}. \tag{2}$$

In Eq. (2) $M_{\max}$ corresponds to the M value in pure first-stage GIC. In the experiment under consideration (the HOPG plate width $l \sim 2\delta_c$) CESR signal intensity I^* increases as the amount of intercalate molecules in the sample increases, i.e., $I^* \propto M$. The problem of choice for $\mu(\tau)$ dependence, which is necessary for the $I^*(\tau)$ calculation with Eq. (2), is a nontrivial one. In the present paper, as well as Alstrom [31], we carried out the simulation of intercalation process with introducing a dependence of the chemical potential μ on time. It was assumed that during intercalation the GIC system passes through a set of quasi-equilibrium states. The reason for such assumption was the following: in the considered experiment the intercalation process is slow enough and the lifetime of definite stage greatly exceeds the duration of transitions between stages (Fig. 1b).

The reason for using in calculation of equilibrium states the analytical Eqs. (1) by Kirczenow [30] instead of those by Alstrom [31] in the frameworks of "devil's staircase" model, is the fact that Eqs. (1) take into account stage disorder phenomena. These phenomena are of importance in stage transitions [30], as confirmed by the numerical calculations of intercalation kinetics [32].

On the basis of the foregoing qualitative considerations the following procedure was used to obtain the dependence $\mu(\tau)$ corresponding to our experimental conditions. The threshold values of the chemical potential, μ_i, which correspond to the stage transitions from stages with index $(i + 1)$ to those with index i, were calculated with Eqs. (1). Corresponding threshold time values τ_i have been determined from experiment. The results of such calculations are presented in Fig. 4.

The dependence $\mu_i(\tau_i)$ for our experiment (Fig. 4) qualitatively differs from that adopted by Alstrom [31] $\mu(\tau) = \mu_\infty[1 - \exp(-\tau/\tau^*)]$, where μ_∞ is the μ value at $\tau \to \infty$, τ^* is the "relaxation" time. Probably, the reason for such deviation is the fact that aforementioned simple relaxation function is a good approximation for large exposure time only (see below). Therefore, we have used a more general expression for $\mu(\tau)$ dependence:

$$\mu(\tau) = p'(\tau)\mu'(\tau) + p''(\tau)\mu''(\tau), \tag{3a}$$

with

$$\mu'(\tau) = a\tau^\beta, \tag{3b}$$

and

$$\mu''(\tau) = \mu_\infty[1 - \exp(-\tau/\tau^*)], \tag{3c}$$

where a and β are some real numbers, $p'(\tau)$ and $p''(\tau)$ are the weight functions, meeting the condition: $p'(\tau) + p''(\tau) \equiv 1$.

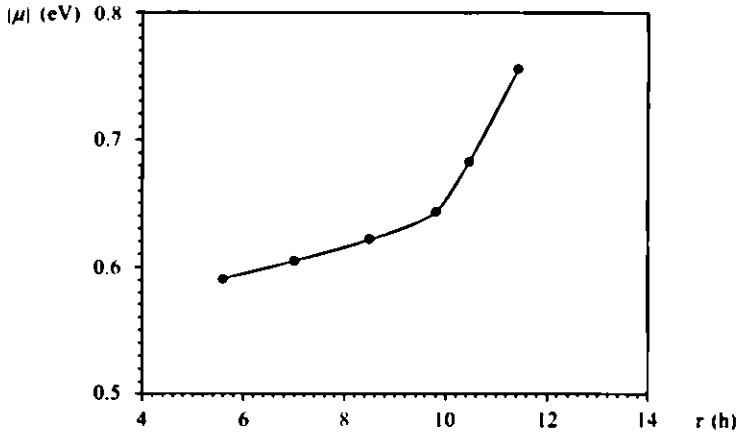

Fig. 4. Chemical potential of the narrow ($l \sim 2\delta_c$) HOPG plate, μ, vs. exposure time, τ, in HNO_3 atmosphere. Dots correspond to the threshold values μ_i and τ_i; solid line corresponds to the theoretical curve (Eqs. (3)).

In Eqs. (3) the first term is dominating during the initial stages of intercalation, which are characterized by necessity of considerable pristine graphite deformation. The second term becomes dominating for the stages with low indices at the large time values. The formation of these stages requires large intercalate amount and, therefore, time. For these reasons functions $p'(\tau)$ and $p''(\tau)$ have been chosen as follows:

$$p'(\tau) = \exp(-\tau/\tau_0),$$

and

$$p''(\tau) = 1 - \exp(-\tau/\tau_0),$$

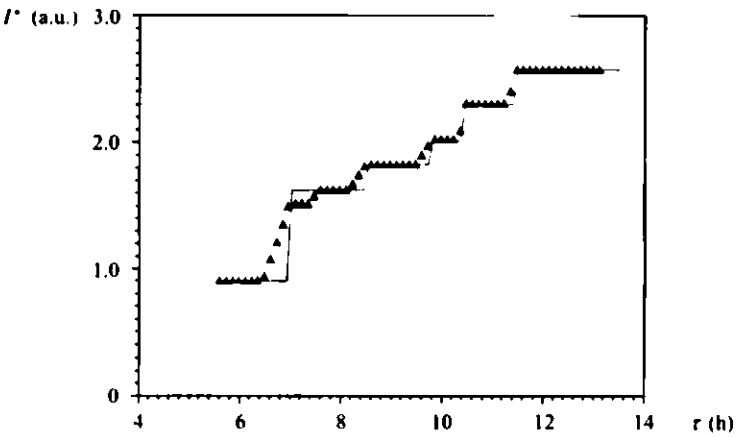

Fig. 5. Experimental (triangles) and the calculated (solid line) integral intensity, I^*, of the CESR signal from intercalated HOPG plate vs. exposure time, τ, in HNO_3 atmosphere.

where τ_0 is the characteristic time at which transition from one mechanism to another takes place. In our case (Fig. 2) τ_0 is about 10 h. The calculation results for $I^*(\tau)$ in the frameworks of the above-stated model (with the set of parameters [30]: $N_0 = 300$, $zE_{//} = 1$ eV, $\gamma = 1$ eV, $\upsilon_0 = 0.3$ eV, $\alpha = 1$) are shown in Fig. 5 and demonstrate a good agreement with experiment.

5 Conclusion

Graphite intercalation by HNO_3 molecules and stage transformations have been studied by CESR technique on HOPG plate with width comparable with the graphite skin-depth governed by the c-axis conductivity. As a result, the significant broadening of the graphite CESR signal during transport of the intercalate through the initial graphite sample and the stepwise changes in the intensity of the intercalated graphite CESR signal on exposure time in HNO_3 atmosphere have been clearly detected. Theoretical consideration for the time evolution of CESR parameters of signals both from nonintercalated and intercalated regions of sample has been carried out. A new form for the dependence of chemical potential vs. exposure time has been introduced with arguments presented, resulting in a successful description of the experimental dependence of the CESR signal intensity from intercalated graphite. The broadening of graphite CESR signal during the advance of the intercalation front into the initial graphite sample is explained by nonzero probability of spin reorientation during collisions of current carriers with the interface between the intercalated and the nonintercalated parts of the plate. Similar experimental and theoretical investigations of graphite intercalation by other intercalants are in progress.

Acknowledgements

The authors are grateful to L. B. Nepomnyashchii (Scientific Research Centre for Graphite, Moscow) for providing the HOPG and to N. M. Mishchenko and V. V. Sereda for help in experiments. This work was supported by the Russian Foundation for Basic Research (grant no. 97-03-33346).

References

1. Dresselhaus M.S., Dresselhaus G.: Adv. Phys. 30, 139–326 (1981)
2. Solin S.A., Zabel H.: Adv. Phys. 37, 87–254 (1988)
3. Lagrange P., Herold A., Herold C.: Mol. Cryst. Liq. Cryst. 310, 33–41 (1998)
4. Davidov R., Milo O., Palchan I., Selig H.: Synth. Met. 8, 83–87 (1983)
5. Palchan I., Davidov D., Zevin V., Polatsek G., Selig H.: Phys. Rev. B 32, 5554–5557 (1985)
6. Palchan I., Mustachi F., Davidov D., Selig H.: Synth. Met. 10, 101–116 (1984/85)
7. Nakajima M., Kawamura K., Tsuzuku T.: J. Phys. Soc. Jpn. 57, 1572–1575 (1988)
8. Ziatdinov A.M., Tsvetnikov A.K., Mishchenko N.M., Sereda V.V.: Mat. Sci. Forum 91/93, 583–588 (1992)
9. Ziatdinov A.M., Mishchenko N.M.: J. Phys. Chem. Solids 58, 1167–1172 (1997)

10. Dyson F.J.: Phys. Rev. 98, 349–359 (1955)
11. Ziatdinov A.M., Mishchenko N.M.: Phys. Solid State (Russia) 36, 1283–1289 (1994)
12. Zevin V., Suss J.T.: Phys. Rev. B 34, 7260–7270 (1986)
13. Kodera H.: J. Phys. Soc. Jpn. 28, 89–98 (1970)
14. Saint Jean M., McRae E.: Phys. Rev. B 43, 3969–3974 (1991)
15. Ziatdinov A.M., Kainara V.V., Krivoshei A.N.: Mol. Cryst. Liq. Cryst., in press.
16. Spain I.L.: Chemistry and Physics of Carbon, vol. 8, p. 119. New York: Marcel Dekker 1973.
17. Walker M.B.: Phys. Rev. B 3, 30–41 (1971)
18. Zhikarev V.A., Kessel A.P., Harahashyan E.G., Cherkasov F.G., Shvarz K.K.: Sov. Phys. JETP 64, 1356–1366 (1973)
19. Nixon D.E., Parry G.S.: J. Phys. D 1, 291–293 (1968)
20. Falardeau E.R., Hanlon L.R., Thompson T.E.: Inorg. Chem. 17, 301–308 (1978)
21. Nishitani R., Uno Y., Suematsu H.: Synth. Met. 7, 13–19 (1983)
22. Misenheimer M.E., Zabel H.: Phys. Rev. Lett. 54, 2521–2524 (1985)
23. Nishitani R., Nishina Y., Hashimoto S., Iwasaki H.: Synth. Met. 12, 161–166 (1985)
24. Nishitani R., Sasaki Y., Nishina Y.: J. Phys. Soc. Jpn. 56, 1051–1057 (1987)
25. Safran S.A.: Solid State Phys. 40, 183–246 (1987)
26. Winokur M.J., Clarke R.: Phys. Rev. Lett. 56, 2072–2075 (1986)
27. Nixon D.E., Parry G.S., Ubbelohde A.R.: Proc. R. Soc. London A 291, 324–334 (1966)
28. Parry G.S.: Mater. Sci. Eng. 31, 99–104 (1977)
29. Shaked H., Pinto H., Melamud M.: Phys. Rev. B 35, 838–843 (1987)
30. Kirczenow G.: Phys. Rev. B 31, 5376–5386 (1985)
31. Alstrom P.: Solid State Commun. 56, 1047–1050 (1985)
32. Kirczenow G.: Phys. Rev. Lett. 55, 2810–2813 (1985)

Authors' address: Albert M. Ziatdinov, Institute of Chemistry, Russian Academy of Sciences, 159, Prosp. 100-letiya, 690022 Vladivostok, Russian Federation